Measuring High-Order Phonon Correlations in an Optomechanical Resonator

Y. S. S. Patil [1,*] J. Yu,[2] S. Frazier,[1] Y. Wang,[2] K. Johnson,[1] J. Fox,[1] J. Reichel,[3] and J. G. E. Harris[1,2,4,†]

[1]*Department of Physics, Yale University, New Haven, Connecticut 06520, USA*
[2]*Department of Applied Physics, Yale University, New Haven, Connecticut 06520, USA*
[3]*Laboratoire Kastler Brossel, ENS-Université PSL, CNRS, Sorbonne Université,*
Collège de France 24 rue Lhomond, 75005 Paris, France
[4]*Yale Quantum Institute, Yale University, New Haven, Connecticut 06520, USA*

We use single photon detectors to probe the motional state of a superfluid ^{4}He resonator of mass ~ 1 ng. The arrival times of Stokes and anti-Stokes photons (scattered by the resonator's acoustic mode) are used to measure the resonator's phonon coherences up to the fourth order. By postselecting on photon detection events, we also measure coherences in the resonator when ≤ 3 phonons have been added or subtracted. These measurements are found to be consistent with predictions that assume the acoustic mode to be in thermal equilibrium with a bath through a Markovian coupling.

Cavity optomechanical systems offer a platform for merging the advantageous features of the optical and the acoustic domains. In the last two decades, coherently coupled optical and acoustic resonators have been used to realize a range of quantum technologies including transducers, sensors, repeaters and memories. Quantum optomechanical devices can also be used in gravitational wave detection, tests of quantum mechanics at macroscopic scales, and searches for physics beyond the standard model [1–9].

To date, most quantum optomechanical devices have operated in a regime where linear equations of motion accurately describe the optical and mechanical modes, the coupling between them, the drives applied to them, and the quantum backaction of their readout. A number of important results have been achieved in this linear regime, including the preparation of mechanical resonators in the ground state and squeezed states [10–13]. However, systems that exhibit nonlinearity at the single quantum level can provide access to states that offer advantages in quantum information processing, and which exhibit the most striking features of quantum mechanics, such as Wigner-function negativity, or violations of Bell-type inequalities [14–17].

One approach to attaining single-quantum nonlinearity is to use the measurement backaction of a single photon detector (SPD) [18,19]. To date, this approach has been used in the domains of quantum optics, cavity QED, and optomechanics [20–27]. In single-mode optomechanical systems, where acoustically scattered photons can be attributed to a single mechanical mode, the detection of a scattered photon heralds the creation (or annihilation) of a phonon in that mechanical mode. Such heralded protocols have been used to measure nonclassical effects in

mechanical resonators with mass ~ 1 pg [28–31]. In devices with mass ~ 1 ng, this approach has been used to measure simpler quantum effects (such as sideband asymmetry), and to verify the thermal character of the two-phonon correlations in the resonator [32].

In this work, single photon detection is used to probe and control (via postselection) the mechanical state of a ~ 1 ng oscillator comprised of superfluid ^{4}He. The oscillator's phonon coherences are measured up to the fourth order, and are found to be consistent with the acoustic mode having a Markovian coupling to its bath. The phonon coherences of k-phonon-subtracted (and k-phonon-added) thermal states are also measured for $k \leq 3$. These results provide a detailed characterization of the acoustic mode's environment, and demonstrate that superfluid mechanical elements are well suited for accessing nonlinear quantum optomechanical effects at the nanogram scale. Several factors contribute to these devices' performance, including their simple geometry, the unique material properties of superfluid ^{4}He, and the wide applicability of SPD-induced backaction [33–35].

Figure 1(a) shows a schematic of the device used here (also described in detail in Ref. [34]). Two single-mode optical fibers with high-reflectivity mirrors fabricated on their end faces are aligned using glass ferrules to form a Fabry-Perot optical cavity. The ferrules and fibers are epoxied to a copper housing that is thermally anchored to the mixing chamber (MC) of a dilution refrigerator at temperature $T_{MC} \approx 20$ mK, and the cavity is filled with superfluid ^{4}He via a capillary line. The fiber mirrors set equivalent boundary conditions for the cavity's optical and acoustic modes (the latter are density waves in the ^{4}He); as a result, these modes' spatial profiles are well approximated by a common set of orthogonal functions (the well-known
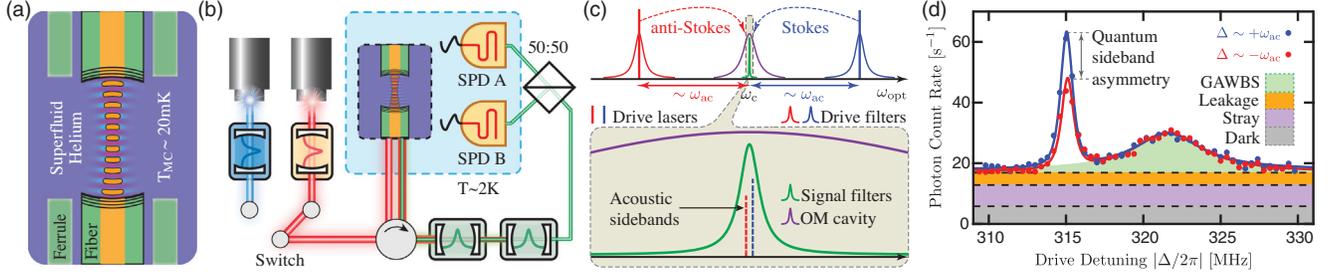
FIG. 1. (a) Device schematic: A fiber-based Fabry-Perot cavity is filled with superfluid ^{4}He. Blue shading denotes the instantaneous ^{4}He density in an acoustic mode. Orange denotes the optical mode intensity. (b) Optical schematic showing the two drive lasers (red and blue paths), optomechanical cavity (OMC, black dashed box), acoustically scattered photons (green path), two signal filter cavities (green), and the two SPDs. The filter cavities (red and blue) before the OMC are used to suppress laser phase noise. (c) Optical spectrum showing the frequencies of the lasers, scattered photons, and filters, all with respect to the OMC's optical resonance. (d) Photon count rate spectrum measured as a function of the drive laser detuning Δ, with $P_{\text{in}} = 400$ nW.

Gaussian modes of paraxial cavities). Since the optome-chanical coupling is set by the overlap of the superfluid density fluctuations with the optical intensity, the ortho-gonality of these modes' spatial profiles ensures an unusu-ally clean realization of single-mode optomechanics: a given optical mode with wavelength λ_c (in ^{4}He) couples only to the acoustic mode with wavelength $\lambda_{\text{ac}} = \lambda_c/2$.

When the optical mode is driven by a laser, the single-mode optomechanical interaction is described by the line-arized Hamiltonian $\mathcal{H}_{\text{OM}} = -\hbar g_0 \sqrt{n_c}(a + a^\dagger)(b + b^\dagger)$, where a and b are the annihilation operators of the optical mode and of the acoustic mode, respectively, n_c is the mean photon number in the cavity, and g_0 is the single photon optomechanical coupling rate [2].

A schematic of the experiment is shown in Figs. 1(b) and 1(c). The optomechanical cavity has an optical resonance at $\omega_c/2\pi = c/(n_{\text{He}}\lambda_c)$ [corresponding to a vacuum wave-length $n_{\text{He}}\lambda_c = 1548.3(1)$ nm] and a linewidth $\kappa_c/2\pi = 47.2(5)$ MHz, where $n_{\text{He}} = 1.0261$ is the refractive index of ^{4}He. It is driven with a laser which is either red-detuned from ω_c by $\Delta \sim -\omega_{\text{ac}}$, or else blue-detuned by $\Delta \sim +\omega_{\text{ac}}$, where $\omega_{\text{ac}}/2\pi = \nu_{\text{He}}/\lambda_{\text{ac}}$ is the acoustic mode frequency and $\nu_{\text{He}} = 238$ m/s is the speed of sound in ^{4}He. The red-(blue-) detuned drive effectively realizes a beam splitter (two-mode squeezing) optomechanical interaction via cav-ity-enhanced anti-Stokes (Stokes) scattering [2]. Photons leaving the cavity (both the unshifted drive photons and the resonant anti-Stokes or Stokes photons) are then incident on two cavities which are arranged in series and have linewidths $\kappa_{\text{FC1}}/2\pi = 1.71(2), \kappa_{\text{FC2}}/2\pi = 1.21(5)$ MHz. These cavities' resonances are locked to ω_c [36]. Since they meet the condition $\gamma_{\text{ac}} \ll \kappa_{\text{FC1,2}}$ (where the acoustic mode's linewidth $\gamma_{\text{ac}}/2\pi \approx 3.5$ kHz) they serve as filters by reflecting the drive photons while passing the anti-Stokes or Stokes photons to superconducting nanowire SPDs.

Figure 1(d) shows a typical measurement of the photon detection rate as a function of Δ. The peaks at $\Delta/2\pi = \mp\omega_{\text{ac}}/2\pi = \mp 315.3(1)$ MHz correspond to the anti-Stokes (Stokes) sidebands of the acoustic mode. This frequency is

consistent with the expected $\omega_{\text{ac}} = 315.40(2)$ MHz for the optical resonance employed [$\lambda_{\text{ac}} = \lambda_c/2 = 754.46(5)$ nm]. The broad peak at $\Delta/2\pi = \mp 322.3(1)$ MHz is caused by guided acoustic wave Brillouin scattering (GAWBS) of drive laser photons in the room temperature optical fibers [48]. A detuning-independent background is also evident. The solid lines in Fig. 1(d) are a fit to the sum of a constant (corresponding to the background counts), a broad Lorentzian (corresponding to the GAWBS signal), and the filter cavities' passband (a product of two Lorentzians, corresponding to the counts from the acoustic sidebands). A detailed description of this fit is given in Ref. [36].

Fits as in Fig. 1(d) yield the optomechanical scattering rates $R_{\text{AS(S)}} = \gamma_{\text{AS(S)}} \times \eta_\kappa \times \eta_{\text{det}}$, where $\gamma_{\text{AS(S)}}$ is the anti-Stokes (Stokes) scattering rate for $\Delta = -\omega_{\text{ac}}$ ($\Delta = +\omega_{\text{ac}}$), $\eta_\kappa = \kappa_{\text{in}}/\kappa_c$ is the cavity coupling efficiency, κ_{in} is the cavity's coupling rate, and η_{det} is the detection efficiency (set by the transmission of the filter cavities and the beam path, and by the SPD quantum efficiency). Standard quan-tum optomechanics theory predicts that $\gamma_{\text{AS}} = \gamma_{\text{ac}}Cn_{\text{ac}}$ and $\gamma_{\text{S}} = \gamma_{\text{ac}}C(n_{\text{ac}} + 1)$, where γ_{ac} is the "bare" acoustic damp-ing rate, $C = 4[(g_0^2)/(\kappa_c\gamma_{\text{ac}})]n_c$ is the multiphoton cooper-ativity [2], and $n_{\text{ac}} = \langle b^\dagger b \rangle$. The difference between $R_{\text{AS}} \propto n_{\text{ac}}$ and $R_{\text{S}} \propto (n_{\text{ac}} + 1)$ is known as the quantum sideband asymmetry (QSA).

As shown in Ref. [36], measurements of R_{AS} and R_{S} indi-cate that the acoustic mode's temperature $T \approx T_{\text{MC}}$ when the incident laser power $P_{\text{in}} \lesssim 300$ nW. Measurements with $P_{\text{in}} > 300$ nW show the standard optomechanical damping effect, as well as heating (due to absorption of photons in the fibers and mirror coatings) that is consistent with a simple thermal model of the device.

Measurements of the mean photon flux [as in Fig. 1(d)] provide information that could also be obtained by hetero-dyne measurements of the acoustic sidebands [2]. However, much richer information is contained in the photon arrival times registered by the SPDs. This is because each detec-tion of an anti-Stokes (Stokes) photon corresponds to the subtraction (addition) of a phonon in the acoustic mode.

For example, the coherence of anti-Stokes photons $g_{\mathrm{AS}}^{(n)} = \langle (a_{\mathrm{AS}}^{\dagger})^n a_{\mathrm{AS}}^n \rangle / \langle a_{\mathrm{AS}}^{\dagger} a_{\mathrm{AS}} \rangle^n$ is equal to the normally ordered phonon coherence $g_{\mathrm{ac}}^{(n)} \equiv \langle (b^{\dagger})^n b^n \rangle / \langle b^{\dagger} b \rangle^n$, while the coherence of Stokes photons $g_{\mathrm{S}}^{(n)} = \langle (a_{\mathrm{S}}^{\dagger})^n a_{\mathrm{S}}^n \rangle / \langle a_{\mathrm{S}}^{\dagger} a_{\mathrm{S}} \rangle^n$ is equal to the antinormally ordered phonon coherence $h_{\mathrm{ac}}^{(n)} \equiv \langle b^n (b^{\dagger})^n \rangle / \langle b b^{\dagger} \rangle^n$ [36]. Here a_{AS} and a_{S} are the annihilation operators for anti-Stokes and Stokes photons, respectively.

Measurements of these phonon coherences can be used to probe the acoustic oscillator's dynamics. For example, an oscillator in a thermal state should exhibit phonon bunching that decays on a timescale set by the oscillator's damping.

If the coupling to the bath is Markovian, then the nth-order coherence is predicted to be $g_{\mathrm{ac}}^{(n)}(\boldsymbol{\tau}) = 1 + f_n(\bar{\gamma}_{\mathrm{ac}} \boldsymbol{\tau})$, where $\boldsymbol{\tau} = (\tau_1, \ldots, \tau_{n-1})$, τ_k is the delay between the kth and $(k+1)$th detected phonon, and the oscillator's total damping rate is $\bar{\gamma}_{\mathrm{ac}}(P_{\mathrm{in}}) = \gamma_{\mathrm{ac}} + \gamma_{\mathrm{opt}}(P_{\mathrm{in}})$, where $\gamma_{\mathrm{opt}}(P_{\mathrm{in}})$ is the contribution from optomechanical backaction [36]. The functions f_n are straightforward to calculate, with $f_2(x) = e^{-x}$ and $f_3(\mathbf{x}) = e^{-x_1} + e^{-x_2} + 3e^{-x_1-x_2}$ [an expression for $f_4(\mathbf{x})$ is given in Ref. [36]].

To measure the optical coherences (and thus the phonon coherences), a histogram of the delays between n photon arrival times $C_{\mathrm{AS(S)}}^{(n)}(\boldsymbol{\tau})$ is constructed and then normalized by its value at large delays. In the experiment, the photon

arrivals registered by the SPDs include the sideband photons as well as other events [such as background photons and dark counts, see Fig. 1(d)]. These extraneous events are measured to be independent and identically distributed over time, so their contribution to $C_{\mathrm{AS(S)}}^{(n)}(\boldsymbol{\tau})$ can be calculated and corrected for [36]. The corrected histograms are fit to the form $A + B \times f_n(\bar{\gamma}_{\mathrm{ac}} \boldsymbol{\tau})$, where A, B, and $\bar{\gamma}_{\mathrm{ac}}$ are fit parameters. The best-fit value of A is used to normalize $C_{\mathrm{AS(S)}}^{(n)}(\boldsymbol{\tau})$ and convert it to the corresponding phonon coherence [i.e., $g_{\mathrm{ac}}^{(n)}(\boldsymbol{\tau}) = C_{\mathrm{AS}}^{(n)}(\boldsymbol{\tau})/A$ and $h_{\mathrm{ac}}^{(n)}(\boldsymbol{\tau}) = C_{\mathrm{S}}^{(n)}(\boldsymbol{\tau})/A$].

Figure 2 shows the phonon coherences measured in this way (up to the fourth order) as a function of delay times, along with the corresponding fits. The zero-delay coherence values extracted from these fits are $g_{\mathrm{ac}}^{(2)}(0) = 1.980(2)$, $h_{\mathrm{ac}}^{(2)}(0) = 2.007(1)$, $g_{\mathrm{ac}}^{(3)}(\mathbf{0}) = 5.843(7)$, $h_{\mathrm{ac}}^{(3)}(\mathbf{0}) = 6.023(2)$, $g_{\mathrm{ac}}^{(4)}(\mathbf{0}) = 23.01(3)$, and $h_{\mathrm{ac}}^{(4)}(\mathbf{0}) = 23.98(1)$ (where the stated uncertainty corresponds to one standard deviation of the best-fit parameter). These values are consistent with the predictions for a thermal state: $g_{\mathrm{ac}}^{(n)}(\mathbf{0}) = h_{\mathrm{ac}}^{(n)}(\mathbf{0}) = n!$. [The fourth-order data and fits shown in Fig. 2(c) are for a finite delay bin of $5\ \mu s < \tau_1 < 15\ \mu s$, and are thus expected to be less than $4! = 24$ for $(\tau_2, \tau_3) \to (0, 0)$.] The $\boldsymbol{\tau}$ dependence of the coherences also agrees well with theory, as evidenced by
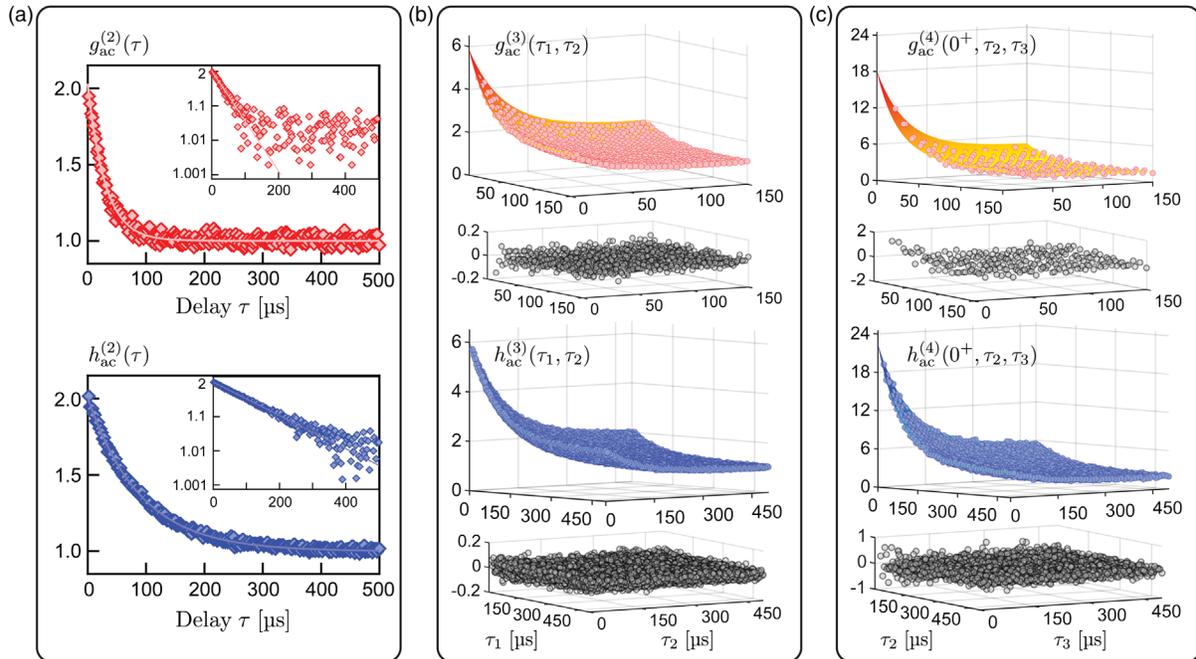
FIG. 2. Phonon coherences: (a) The second-, (b) third-, and (c) fourth-order phonon coherences measured for $P_{\mathrm{in}} \approx 5\ \mu W$, with photon arrival times binned in 2, 5, and 10 μs bins, respectively. In (a), the insets show the same data on a logarithmic scale. For the three-time dependent $g_{\mathrm{ac}}^{(4)}(\tau_1, \tau_2, \tau_3)$ and $h_{\mathrm{ac}}^{(4)}(\tau_1, \tau_2, \tau_3)$, we only show representative 2D slices of $g_{\mathrm{ac}}^{(4)}(0^+, \tau_2, \tau_3)$ and $h_{\mathrm{ac}}^{(4)}(0^+, \tau_2, \tau_3)$, where $\tau = 0^+$ represents the bin with $5\ \mu s < \tau < 15\ \mu s$. See Ref. [36] for other 2D slices. Solid lines or surfaces show the fits described in the text. Fits for (c) are to the entire 3D (i.e., τ_1-, τ_2-, τ_3-dependent) dataset. Fit residuals are shown in black for (b) and (c).
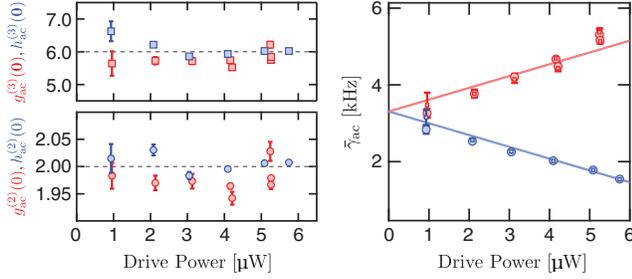
FIG. 3. The zero-delay second- and third-order coherences, and the coherence decay rates ($\bar{\gamma}_{ac}$), as a function of incident power P_{in}. Data is extracted from fits to the second-order (circles) and third-order (squares) coherences. Solid lines show a fit to standard optomechanics theory.

FIG. 4. (a) Dynamics of the mean phonon occupancy upon subtraction or addition of k phonons at $\tau = 0$. (b) Second order coherences of a 1-phonon subtracted (red) and added (blue) thermal state. Solid lines show the theoretical predictions, see Ref. [36]. Data shown for $P_{in} \approx 5~\mu W$.

the small residuals. This demonstrates that the acoustic mode is in equilibrium with the bath and that its energy fluctuations are consistent with a Gaussian distribution (to at least the fourth cumulant).

Figure 3 shows various features of these fits for $0.9~\mu W < P_{in} < 6~\mu W$ (corresponding to $1 \lesssim n_{ac} \lesssim 10$ [36]). The left panel shows that the zero-delay second- and third-order coherences are close to 2 and 6, respectively, for all P_{in} in this range. The right panel shows that the decay rates $\bar{\gamma}_{ac}(P_{in})$ extracted from fits (as in Fig. 2) exhibit the expected optomechanical backaction. A fit to standard optomechanics theory [2] (solid lines) gives $g_0/2\pi = 4.70(5)$ kHz, consistent with the independent calibration described in Ref. [36].

The analysis described above (and shown in Figs. 2 and 3) utilizes all the photons registered by the SPD. However, by post-selecting data that is recorded immediately after detection of one or more anti-Stokes (Stokes) photons, one can measure the properties of phonon-subtracted (phonon-added) states. For instance, $g_{ac}^{(2)}(0) = 2$ implies that the mean rate of photon arrivals doubles immediately after the detection of one anti-Stokes photon (or, equivalently, the subtraction of a phonon). As the scattering rate γ_{AS} is proportional to the acoustic mode's mean phonon occupancy n_{ac}, one can conclude that n_{ac} doubles after the subtraction of a phonon. More generally, the evolution of the mean phonon occupancy $n_{ac}^{-k}(\tau)$ [$n_{ac}^{+k}(\tau)$] of a k-phonon subtracted (added) state can be measured through appropriate postselection [36].

Measurements for $k = 1, 2, 3$ are shown in Fig. 4(a). If the equilibrium state (i.e., the state before the k-phonon subtraction or addition event) is thermal, $n_{ac}^{-k}(0) = (k + 1)n_{ac}$, i.e., the mean occupancy increases $(k + 1)$-fold on the subtraction of k phonons, while $n_{ac}^{+k}(0) = (k + 1)n_{ac} + k$. This seemingly counter intuitive form of the increase in n_{ac} can be understood as a Bayesian update to the thermal state. Viewed in the Fock basis, the detection of a scattered photon from a thermal state is more likely to occur from its high-n Fock components than from its small-n Fock components, and this biases the probability distribution toward high n
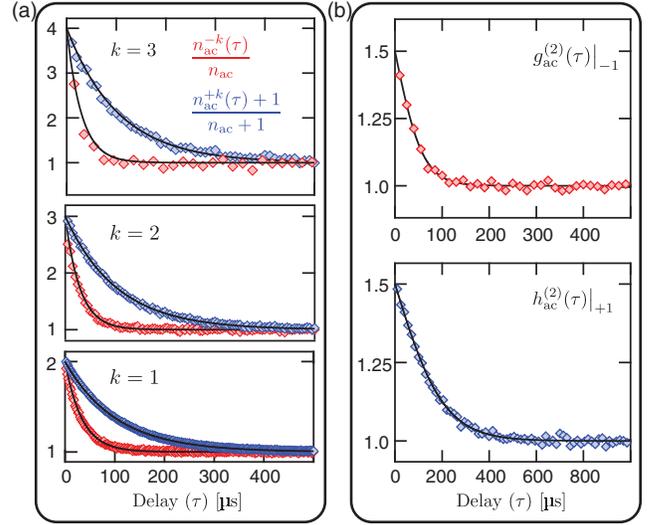
[36]. As seen in Fig. 4(a), the phonon occupancy is indeed measured to double, triple, or quadruple immediately after 1, 2, or 3-phonon subtraction, and to subsequently decay back to equilibrium occupancy with the predicted time dependence (solid lines).

Similarly, we construct the various coherences of the heralded k-phonon subtracted (or added) thermal states through appropriate postselection. The nth order coherences of such heralded states are determined by various slices in the higher-dimensional $(n + k)$-photon detection record. While this record viewed as a whole corresponds to that of a thermal state, the postselection extracts the nonthermal heralded state coherences [36]. Figure 4(b) shows the measured second-order coherence of a 1-phonon subtracted thermal state [normally ordered $g_{ac}^{(2)}(\tau)|_{-1}$], and of a 1-phonon added thermal state [antinormally ordered $h_{ac}^{(2)}(\tau)|_{+1}$], along with their theoretical expectations (solid lines). The measured zero-time second order coherences agree well with the theoretical expectation of 3/2, as does their decay to unity on the mechanical timescale.

Coherences and other statistics of k-quanta -subtracted or -added thermal states are of interest in quantum metrology, quantum information and quantum thermodynamics. The optical equivalents of such states have been shown to be efficient at performing work and carrying information [49]. The ability to create and probe these states in an acoustic mode, as demonstrated here, extends the potential use of such states to optomechanical platforms [50–52].

---

[*] yogesh.patil@yale.edu
[†] jack.harris@yale.edu

[1] P. Meystre, A short walk through quantum optomechanics, Ann. Phys. (Berlin) **525**, 215 (2013).

[2] M. Aspelmeyer, T. J. Kippenberg, and F. Marquardt, Cavity optomechanics, Rev. Mod. Phys. **86**, 1391 (2014).

[3] G. Kurizki, P. Bertet, Y. Kubo, K. Mølmer, D. Petrosyan, P. Rabl, and J. Schmiedmayer, Quantum technologies with hybrid systems, Proc. Natl. Acad. Sci. U.S.A. **112**, 3866 (2015).

[4] W. P. Bowen and G. J. Milburn, *Quantum Optomechanics* (CRC Press, Boca Raton, 2015).

[5] M. Metcalfe, Applications of cavity optomechanics, Appl. Phys. Rev. **1**, 031105 (2014).

[6] D. Carney *et al.*, Mechanical quantum sensing in the search for dark matter, Quantum Sci. Technol. **6**, 024002 (2021).

[7] O. Romero-Isart, A. C. Pflanzer, F. Blaser, R. Kaltenbaek, N. Kiesel, M. Aspelmeyer, and J. I. Cirac, Large Quantum Superpositions and Interference of Massive Nanometer-Sized Objects, Phys. Rev. Lett. **107**, 020405 (2011).

[8] A. D. Cronin, J. Schmiedmayer, and D. E. Pritchard, Optics and interferometry with atoms and molecules, Rev. Mod. Phys. **81**, 1051 (2009).

[9] M. Arndt, A. Ekers, W. von Klitzing, and H. Ulbricht, Focus on modern frontiers of matter wave optics and interferometry, New J. Phys. **14**, 125006 (2012).

[10] J. Chan, T. P. M. Alegre, A. H. Safavi-Naeini, J. T. Hill, A. Krause, S. Gröblacher, M. Aspelmeyer, and O. Painter, Laser cooling of a nanomechanical oscillator into its quantum ground state, Nature (London) **478**, 89 (2011).

[11] J. D. Teufel, T. Donner, D. Li, J. W. Harlow, M. S. Allman, K. Cicak, A. J. Sirois, J. D. Whittaker, K. W. Lehnert, and R. W. Simmonds, Sideband cooling of micromechanical motion to the quantum ground state, Nature (London) **475**, 359 (2011).

[12] E. E. Wollman, C. U. Lei, A. J. Weinstein, J. Suh, A. Kronwald, F. Marquardt, A. A. Clerk, and K. C. Schwab, Quantum squeezing of motion in a mechanical resonator, Science **349**, 952 (2015).

[13] C. F. Ockeloen-Korppi, E. Damskägg, J. M. Pirkkalainen, M. Asjad, A. A. Clerk, F. Massel, M. J. Woolley, and M. A. Sillanpää, Stabilized entanglement of massive mechanical oscillators, Nature (London) **556**, 478 (2018).

[14] J. C. Matthews, X.-Q. Zhou, H. Cable, P. J. Shadbolt, D. J. Saunders, G. A. Durkin, G. J. Pryde, and J. L. O'Brien, Towards practical quantum metrology with photon counting, npj Quantum Inf. **2**, 16023 (2016).

[15] K. C. Tan and H. Jeong, Nonclassical light and metrological power: An introductory review, AVS Quantum Sci. **1**, 014701 (2019).

[16] D. R. M. Arvidsson-Shukur, N. Yunger Halpern, H. V. Lepage, A. A. Lasek, C. H. W. Barnes, and S. Lloyd, Quantum advantage in postselected metrology, Nat. Commun. **11**, 3775 (2020).

[17] A. Mari and J. Eisert, Positive Wigner Functions Render Classical Simulation of Quantum Computation Efficient, Phys. Rev. Lett. **109**, 230503 (2012).

[18] E. Knill, R. Laflamme, and G. J. Milburn, A scheme for efficient quantum computation with linear optics, Nature (London) **409**, 46 (2001).

[19] S. Scheel, K. Nemoto, W. J. Munro, and P. L. Knight, Measurement-induced nonlinearity in linear optics, Phys. Rev. A **68**, 032310 (2003).

[20] L. Mandel, Quantum effects in one-photon and two-photon interference, Rev. Mod. Phys. Suppl. **71**, S274 (1999).

[21] L. M. Duan, M. D. Lukin, J. I. Cirac, and P. Zoller, Long-distance quantum communication with atomic ensembles and linear optics, Nature (London) **414**, 413 (2001).

[22] A. Kuzmich, W. P. Bowen, A. D. Boozer, A. Boca, C. W. Chou, L. M. Duan, and H. J. Kimble, Generation of nonclassical photon pairs for scalable quantum communication with atomic ensembles, Nature (London) **423**, 731 (2003).

[23] K. C. Lee, M. R. Sprague, B. J. Sussman, J. Nunn, N. K. Langford, X.-M. Jin, T. Champion, P. Michelberger, K. F. Reim, D. England, D. Jaksch, and I. A. Walmsley, Entangling macroscopic diamonds at room temperature, Science **334**, 1253 (2011).

[24] J. D. Cohen, S. M. Meenehan, G. S. Maccabe, S. Gröblacher, A. H. Safavi-Naeini, F. Marsili, M. D. Shaw, and O. Painter, Phonon counting and intensity interferometry of a nanomechanical resonator, Nature (London) **520**, 522 (2015).

[25] M. D. Anderson, S. Tarrago Velez, K. Seibold, H. Flayac, V. Savona, N. Sangouard, and C. Galland, Two-Color Pump-Probe Measurement of Photonic Quantum Correlations Mediated by a Single Phonon, Phys. Rev. Lett. **120**, 233601 (2018).

[26] B. Hacker, S. Welte, S. Daiss, A. Shaukat, S. Ritter, L. Li, and G. Rempe, Deterministic creation of entangled atom-light Schrödinger-cat states, Nat. Photonics **13**, 110 (2019).

[27] S. T. Velez, K. Seibold, N. Kipfer, M. D. Anderson, V. Sudhir, and C. Galland, Preparation and Decay of a Single Quantum of Vibration at Ambient Conditions, Phys. Rev. X **9**, 041007 (2019).

[28] R. Riedinger, S. Hong, R. A. Norte, J. A. Slater, J. Shang, A. G. Krause, V. Anant, M. Aspelmeyer, and S. Gröblacher, Non-classical correlations between single photons and phonons from a mechanical oscillator, Nature (London) **530**, 313 (2016).

[29] S. Hong, R. Riedinger, I. Marinković, A. Wallucks, S. G. Hofer, R. A. Norte, M. Aspelmeyer, and S. Gröblacher, Hanbury Brown and Twiss interferometry of single phonons from an optomechanical resonator, Science **358**, 203 (2017).

[30] R. Riedinger, A. Wallucks, I. Marinković, C. Löschnauer, M. Aspelmeyer, S. Hong, and S. Gröblacher, Remote quantum entanglement between two micromechanical oscillators, Nature (London) **556**, 473 (2018).

[31] I. Marinković, A. Wallucks, R. Riedinger, S. Hong, M. Aspelmeyer, and S. Gröblacher, Optomechanical Bell Test, Phys. Rev. Lett. **121**, 220404 (2018).

[32] I. Galinskiy, Y. Tsaturyan, M. Parniak, and E. S. Polzik, Phonon counting thermometry of an ultracoherent membrane resonator near its motional ground state, Optica **7**, 718 (2020).

[33] L. A. De Lorenzo and K. C. Schwab, Ultra-high Q acoustic resonance in superfluid ^{4}He, J. Low Temp. Phys. **186**, 233 (2017).

[34] A. B. Shkarin, A. D. Kashkanova, C. D. Brown, S. Garcia, K. Ott, J. Reichel, and J. G. E. Harris, Quantum Optomechanics in a Liquid, Phys. Rev. Lett. **122**, 153601 (2019).

[35] G. S. Agarwal and S. S. Jha, Theory of optomechanical interactions in superfluid He, Phys. Rev. A **90**, 023812 (2014).

[36] See Supplemental Material at http://link.aps.org/supplemental/10.1103/PhysRevLett.128.183601 for details of experimental methods and protocols, fits and theoretical calculations, which includes Refs. [37–47].

[37] N. Takefushi, M. Yoshida, K. Kasai, T. Hirooka, and M. Nakazawa, Gawbs noise characteristics in digital coherent transmission in various optical fibers, in *Proceedings of the 24th OptoElectronics and Communications Conference (OECC) and 2019 International Conference on Photonics in Switching and Computing (PSC)* (IEEE, 2019), pp. 1–3, 10.23919/PS.2019.8818113.

[38] F. Marquardt, J. P. Chen, A. A. Clerk, and S. M. Girvin, Quantum Theory of Cavity-Assisted Sideband Cooling of Mechanical Motion, Phys. Rev. Lett. **99**, 093902 (2007).

[39] A. Kashkanova, Optomechanics with superfluid helium, Ph. D. thesis, Yale University, 2017.

[40] V. Burenkov, H. Xu, B. Qi, R. H. Hadfield, and H.-K. Lo, Investigations of afterpulsing and detection efficiency recovery in superconducting nanowire single-photon detectors, J. Appl. Phys. **113**, 213102 (2013).

[41] M. Fujiwara, A. Tanaka, S. Takahashi, K. Yoshino, Y. Nambu, A. Tajima, S. Miki, T. Yamashita, Z. Wang, A. Tomita, and M. Sasaki, Afterpulse-like phenomenon of superconducting single photon detector in high speed quantum key distribution system, Opt. Express **19**, 19562 (2011).

[42] P. Kelley and W. Kleiner, Theory of electromagnetic field measurement and photoelectron counting, Phys. Rev. **136**, A316 (1964).

[43] K. Børkje, A. Nunnenkamp, and S. M. Girvin, Proposal for Entangling Remote Micromechanical Oscillators via Optical Measurements, Phys. Rev. Lett. **107**, 123601 (2011).

[44] M.-A. Lemonde, N. Didier, and A. A. Clerk, Antibunching and unconventional photon blockade with gaussian squeezed states, Phys. Rev. A **90**, 063824 (2014).

[45] U. Weiss, *Quantum Dissipative Systems*, 4th ed. (World Scientific, Singapore, 2012).

[46] C. W. Gardiner and M. J. Collett, Input and output in damped quantum systems: Quantum stochastic differential equations and the master equation, Phys. Rev. A **31**, 3761 (1985).

[47] R. Loudon, *The Quantum Theory of Light* (Oxford University Press, Oxford, 2000).

[48] R. M. Shelby, M. D. Levenson, and P. W. Bayer, Guided acoustic-wave brillouin scattering, Phys. Rev. B **31**, 5244 (1985).

[49] J. Hloušek, M. Ježek, and R. Filip, Work and information from thermal states after subtraction of energy quanta, Sci. Rep. **7**, 13046 (2017).

[50] G. Enzian, J. J. Price, L. Freisem, J. Nunn, J. Janousek, B. C. Buchler, P. K. Lam, and M. R. Vanner, Single-Phonon Addition and Subtraction to a Mechanical Thermal State, Phys. Rev. Lett. **126**, 033601 (2021).

[51] R. N. Patel, T. P. McKenna, Z. Wang, J. D. Witmer, W. Jiang, R. Van Laer, C. J. Sarabalis, and A. H. Safavi-Naeini, Room-Temperature Mechanical Resonator with a Single Added or Subtracted Phonon, Phys. Rev. Lett. **127**, 133602 (2021).

[52] G. Enzian, L. Freisem, J. J. Price, A. O. Svela, J. Clarke, B. Shajilal, J. Janousek, B. C. Buchler, P. K. Lam, and M. R. Vanner, Non-Gaussian Mechanical Motion via Single and Multiphonon Subtraction from a Thermal State, Phys. Rev. Lett. **127**, 243601 (2021).